

Effect of aqueous medium on low-frequency dynamics, chemical activity and physical properties of a spherical virus

Chetna Tiwari, Vaishali Sharma, Prafulla K. Jha & Arun Pratap

To cite this article: Chetna Tiwari, Vaishali Sharma, Prafulla K. Jha & Arun Pratap (2019): Effect of aqueous medium on low-frequency dynamics, chemical activity and physical properties of a spherical virus, Journal of Biomolecular Structure and Dynamics, DOI: [10.1080/07391102.2019.1626286](https://doi.org/10.1080/07391102.2019.1626286)

To link to this article: <https://doi.org/10.1080/07391102.2019.1626286>



Published online: 08 Jun 2019.



Submit your article to this journal [↗](#)



Article views: 5



View Crossmark data [↗](#)



Effect of aqueous medium on low-frequency dynamics, chemical activity and physical properties of a spherical virus

Chetna Tiwari^{a,b}, Vaishali Sharma^b, Prafulla K. Jha^b and Arun Pratap^a

^aDepartment of Applied Physics, Faculty of Technology and Engineering, The M. S. University of Baroda, Vadodara, India; ^bDepartment of Physics, Faculty of Science, The M.S. University of Baroda, Vadodara, India

Communicated by Ramaswamy H. Sarma

ABSTRACT

In this work, we have studied the effect of size and aqueous medium on the low-frequency dynamics, physical properties like melting temperature and glass transition temperature and chemical properties like catalytic activation energy of spherical virus using Lindemann's criteria and Arrhenius relation under their dynamic limit. The melting temperature and catalytic activation energy decrease with decreasing size of spherical virus. The glass transition temperature which increases with decreasing size of the virus is analyzed through the size dependent melting temperature. The melting temperature and catalytic activation energy of spherical virus of particular size increases when it is embedded in glycerol or water due to mismatch of the physical properties at the interface of virus and surrounding medium. In addition, the glass transition temperature of free and glycerol/water embedded virus using low-frequency vibrational modes has been calculated under the framework of elastic continuum approximation model. The glass transition temperature of spherical virus decreases with size when embedded in glycerol or water. A correlation between T_g and T_m is also drawn for spherical viruses. The study can be useful for spherical virus borne therapy i.e. in detecting and killing of the spherical viruses using a principle based on acoustic phonons (sound waves) resonance.

ARTICLE HISTORY

Received 22 March 2019
Accepted 28 May 2019

KEYWORDS

Virus; lysozyme; catalytic activity; glass transition; low-frequency phonon mode

1. Introduction

The minuscule living organisms viruses and bacteria occur with different shapes and sizes in nature. Nonetheless, most of the viruses tend to be in spherical shapes with diameter ranging amidst 20–100 nm. All viruses are infinitesimal pockets of protein coat (capsid) which encloses nucleic acid core composed of either DNA or RNA. These tiny viruses have found promising applications in several fields of rapidly growing nanotechnologies (Pankhurst, Connolly, Jones, & Dobson, 2003). In past years, the application of biological objects including viruses and bacteria as nanotemplates in nanofabrication was acquired (Alonso, Górzny, & Bittner, 2013; Flynn, Lee, Peelle, & Belcher, 2003; Górzny, Walton, & Evans, 2010; Park et al., 2016; Shenton, Douglas, Young, Stubbs, & Mann, 1999). For instance, tobacco mosaic virus (TMV) and M13 bacteriophage were successfully used in the synthesis of metallic and semiconductor nanowires (Shenton et al., 1999). For nanomaterial's self-assembly, inherently mutated TMV and M13 were well used (Flynn et al., 2003). Furthermore, the physical properties of TMV make it an attractive molecule for engineering hybrid materials (Alonso et al., 2013). Metal-coated TMVs have been used as a structural component in nickel-zinc and lithium ion batteries while TMV coated with fine platinum is a promising anode material for direct methanol fuel cells (Gorzny, Walton, & Evans, 2010). The utilization of viruses commonly occurs in

two categories (i) major fabrication for bulk devices such as energy generation/storage, or ferrofluids; (ii) manufacturing of fine layers or wires for biosensors in the form of small quantity (Alonso et al., 2013). The researchers have successfully used genetically engineered viruses in contrast to the usual high-tech materials or microchips to harvest solar energy (Park et al., 2016). In addition, the common viruses have been found useful in producing materials that resemble skin and bone (Chung et al., 2011). The evaluation of physical and chemical properties of viruses has been extensively explored (Ghavanloo & Fazelzadeh, 2014; May, 2014; Talati & Jha, 2006) and topic of interest due to their budding use in nanotechnology and therapeutics. An insight in their mechanism is gaining many attentions in order to utilize them in nanotechnology (Aggarwal, May, Brooks & Klug, 2016; Lošdorfer Božič & Šiber, 2018; Zhang & Zhang, 2018). Our study will help in making predictions about biological phenomena and determining their properties relevant to nanotechnology design efforts and new therapeutic targets. Through low-frequency vibration analysis one can find its application in diagnosis/treatment of various viral diseases. The concept of killing and destroying viruses can be supported by the Rife therapy performed by a Rife frequency instrument, which destroys the microbe when there is a resonance between the mechanical oscillation frequency. The existence of well-defined resonance has also been emphasized by Ford (2003) for which the knowledge of damping

and width of the resonance is important and could be valuable for science and medicine. Another analogy to this is An Opera Singers voice which can break a thin crystal glass if the signal can match the glass natural frequency.

Production and functioning of viruses can be better when the physical properties such as melting temperature, glass transition temperature and catalytic activation energy are well known both in free and embedded conditions. The study of glass transition temperature (T_g) for nanomaterials has been a subject of extensive attraction from last few years due to their significantly important applications. The particular interest however developed when a depression was first observed for small molecule glass formers confined in nanoporous glasses (Jackson & McKenna, 1991). Nevertheless, there exists reports which claim enhancement in T_g for confined glass formers (Jerome, 1999). Glass transition temperature (T_g) of a material is not only important for its mechanical properties but also for many applications including to know the maximum usable temperature of the material. Furthermore, this is especially important for nanotechnologies that use polymeric thin films, using advanced integrated circuits (Koh, McKenna, & Simon, 2006). It has been found that the finite size of a material affects its glass transition state and solubility (Jiang, Shi, & Li, 1999). Recently, the denatured hen egg white lysozyme, a highly basic protein has been found an effective tool for the solubilization of fullerene (Siepi et al., 2017).

The melting temperature behavior of nanoparticles has attracted notable attentions and has been broadly studied (Dash, 1999; Gupta, Talati & Jha, 2008; Nanda 2009). In several areas, viruses are made to be active and inactive according to their need based applications. In this context, information about the thermodynamical parameter, melting temperature of the virus is important to be known before its application. Recently, Ku et al. (2009) predicted the melting temperature directly from protein sequencing. It is observed that the proteins can be inactivated by high temperature. Hence, an accurate determination of the onset temperature at which proteins are irreversibly inactivated is of great importance to both protein science and the pharmaceutical industries (Zhong, Wang, Ma, & Li, 2016). The protein melting (T_m) is defined as the temperature at which the protein denaturation occurs. The protein denaturation very much depends on its size modification. Protein denaturation comprises an alteration in the protein structure (ordinarily an unfolding) with the loss of activity (Mallamace et al., 2016). The area of nanocatalysis has been an active area of research from past many years (Chen & Kucernak, 2004). The enzyme molecule lowers the activation energy of the reaction and increases its rate (Pauling, 1948). Furthermore, the lysozyme functionalized bioactive glasses which influences the cytotoxicity and anticancer activity have received attention in biomedical applications (Zheng et al., 2016). The efficient protein adsorption and drug delivery capability of bioactive glasses suggest that the size- and medium-dependent catalytic activity of lysozyme can be better utilized in many protein based applications and pharmaceutical industries.

In this paper, we report a systematic study on the size and surrounding dependent melting temperature, catalytic activity and glass transition temperature of a spherical virus using thermodynamical approaches. We also investigated the glass transition temperature using a new approach based on the low-frequency Raman modes calculated under the framework of an elastic continuum model together with the proper boundary conditions at the virus surface. The low-frequency Raman modes of the spherical virus is calculated using the longitudinal and transverse sound speeds c_l and c_t of lysozyme which is similar to the speeds of sound in different protein crystals such as ribonuclease and hemoglobin (Tsen et al., 2006) and successfully used earlier by many researchers (Dykeman, Sankey, & Tsen, 2007; Talati & Jha, 2006). Furthermore, taking lysozyme as the protein coat in spherical virus is justified as it is a known powerful antibacterial protein widely distributed in various biological fluids and tissues including avian egg, plant, bacteria, tears, saliva, milk etc.

2. Methodology

To determine the size and temperature dependent thermodynamical parameters a unique approach based on the thermodynamics using size and shape terms is necessary. In this study, to model the size dependent thermodynamical properties such as melting temperature, catalytic activation energy and glass transition temperature, well-known Arrhenius equation is employed. The size and temperature dependent catalytic activation energy under the framework of Arrhenius equation can be expressed as (Arrhenius, 1889);

$$K(D, T) = K_0(D) \exp\left(\frac{-E_a(D)}{RT}\right) \quad (1)$$

Where K_0 is the pre-exponential factor. $E_a(D)$ expresses size dependent catalytic activation energy, R being the ideal gas constant and T is the temperature. Assuming the same average rate constant at the melting temperature for all viruses, we get the following expression to relate the catalytic activation energy and melting temperature (Lu & Meng, 2010).

$$\frac{E_a(D)}{E_a(\infty)} = \frac{T_m(D)}{T_m(\infty)} \quad (2)$$

Where, $E_a(\infty)$ is catalytic activation energy in bulk form, $T_m(D)$ is size dependent melting temperature and $T_m(\infty)$ is melting temperature of nanometric virus in bulk i.e. lysozyme protein crystal. The expression for the melting temperature of a nanoparticle (virus) embedded in a medium can be written as (Qi & Wang, 2005)

$$\frac{T_m}{T_{mb}} = \left[1 - \frac{3d\alpha}{2D} \left(1 - \frac{T_M}{T_{mb}} \right) \right] \quad (3)$$

Here, T_m is the melting temperature of virus nanoparticle with particular size (diameter), T_{mb} is the melting temperature of virus (lysozyme) in bulk, d is the actual diameter of virus and T_M is the melting temperature of the matrix (encircling medium). The α present in the above equation is shape factor and is considered equal to one for the spherical form.

The comparison of Equations (2) and (3) gives rise to the following expression,

$$T_m = T_m(D) \text{ and } T_{mb} = T_m(\infty) \quad (4)$$

Therefore, the catalytic activation energy using Equation (1) can be written as,

$$E_a(D) = \left[1 - \frac{3d\alpha}{2D} \left(1 - \frac{T_M}{T_{mb}} \right) \right] E_a(\infty) \quad (5)$$

Equations (3) and (5), respectively will provide values of size dependent melting temperature T_m and catalytic activation energy E_a of an embedded spherical virus. These equations clearly reflect the effect of surrounding medium inclusion. Glycerol and water are the most common mediums in which viruses are present. In addition, the approach which will appear in what follows; the low-frequency studies on viruses have been performed with these surrounding mediums. It is clearly seen from above equations that the inclusion of surrounding mediums modifies the expressions of these quantities, which can be attributed to the modification in cohesive energy of the free virus case. As far as low-frequency method for determination of glass transition is concerned, there is a loss of energy in the vibrational modes when it is embedded in mediums. This is introduced in the formulation by incorporating a quantity called specific acoustic impedance which depends on the physical parameters such as density, sound velocities etc. The specific acoustic impedance varies from solvent to solvent; hence the energy loss of the virus vibrational mode will vary. In simple word if there is less mismatch in impedance i.e. acoustic parameters, the energy loss is less. Furthermore, water is a strong IR absorbing medium, and typically, samples can be investigated more successfully by Raman instead of Fourier transform infrared methods while glycerol is generally preferred biological cryopreservants (Farrant, 1970).

According to Lindemann's criterion, a crystal melts when root mean square value of amplitude of thermal vibration (σ) of atoms or molecules reaches a critical fraction of interatomic distances at particular temperature and expressed as (Jiang & Yang, 2008)

$$\sigma^2(r, T) = F(r) T, \quad (6)$$

where $F(r)$ is a size dependent function.

In amorphous solids and glasses, calculations of the thermal conductivity at temperature above 50K are well illustrated with a distinct model, due to Einstein, in which the harmonic motion of nearby atoms is uncorrelated. This model determines an elementary phenomenological depiction of the lattice vibrations in the frequency range of terahertz, and grants a quantifiable explanation of the heat transport. The heat capacity behavior of the glasses studied in the range 5–300K is well described by the combination of Debye and Einstein heat capacity functions (Mamedov et al., 1987). The Lindemann's model developed in 1910 for the study of melting transition is based on Einstein's explanation of the low temperature specific heat of crystals, $c_p(\infty)$ where the corresponding bulk characteristic Einstein temperature $\theta_e(\infty)$ is proportional to the Einstein frequency $\nu_E(\infty)$ as $\hbar\nu_E(\infty) = \theta_e(\infty)$. Here, \hbar is the plank's constant. Lindemann's

criteria has also been successfully applied to describe changes in the local dynamics of protein (Zhou, Vitkup, & Karplus, 1999), atomic clusters (Stillinger & Stillinger, 1990) and polymer melts (Dudowicz, Freed, & Douglas, 2005; Katava et al., 2017).

According to Shi's model for $T_m(r)$, the mean square displacement of a nanoparticle, $\sigma^2(r)$ can be presented as (Shi, 1994);

$$\frac{F(r)}{F(\infty)} = \frac{\{\sigma^2(r, T_m(r)/h^2)\}}{\{\sigma^2(\infty, T_m(\infty)/h^2)\}} \left[\frac{T_m(\infty)}{T_m(r)} \right] = \frac{T_m(\infty)}{T_m(r)} \quad (7)$$

Therefore melting temperature, T_m can be written as;

$$\frac{T_m(r)}{T_m(\infty)} = \frac{\sigma^2(\infty)}{\sigma^2(r)} = \exp \left\{ \frac{-(\alpha-1)}{\left[\left(\frac{r}{r_0} \right) - 1 \right]} \right\} \quad (8)$$

where $\alpha = [2S_{vib}(\infty)/(3R)] + 1$

Since, glasses and crystals as solids have analogs structural characteristics of the short range order, they should possess the similar vibrational characteristics at their melting temperature. The glass transition temperature, T_g is deemed to be second order transition, therefore it can be acquired by substituting $C_{pg}(\infty)$ in place of S_{vib} in Equation (8), where $C_{pg}(\infty)$ is the heat capacity difference between the bulk glass and bulk liquid at $T_g(\infty)$. According to phenomenological observation, it is assumed that the $\sigma_g^2(\infty) \approx \sigma^2(\infty)$, where the subscript g denotes glass transition temperature, T_g . Replacing $T_m(r)$, $T_m(\infty)$, $\sigma^2(r)$ and $\sigma^2(\infty)$ with $T_g(r)$, $T_g(\infty)$, $\sigma_g^2(r)$ and $\sigma_g^2(\infty)$ in Equation (8), we obtain (Lu & Meng, 2010)

$$\frac{T_g(r)}{T_g(\infty)} = \frac{\sigma_g^2(\infty)}{\sigma_g^2(r)} = \exp \left\{ \frac{-(\alpha-1)}{\left[\left(\frac{r}{r_0} \right) - 1 \right]} \right\} \quad (9)$$

$r_0 = c_1(3-d)h$, where d represents dimension; $d=1$ for nanosphere, $d=2$ for nanowires and $d=3$ for thin films. c_1 is the additional condition for different surface states which in case of nanocrystals is equal to unity.

As the virus is in the range of few nanometers like nanoparticles, the wavelength of low-frequency acoustic phonons is related to the atomic spacing, the virus nanoparticle can be treated as a uniform continuum sphere together with the isotropic medium (Zheng et al., 2016). The vibrational modes of a nanometric particle were first calculated by Lamb (1882) by considering the acoustic vibrations of a particle as a whole from classical point of view and later by many others (Duval, 1992; Gupta, Sahoo, Jha, Arora, & Azhniuk, 2009; Talati & Jha, 2006). This requires sphere size, density and sound in corresponding bulk material as parameters to be used in calculation. The low-frequency vibrational modes are of two types: spheroidal and torsional modes. We have calculated the low-frequency vibration of spherical virus as this is analogous to semiconductor nanocrystals or quantum dots. The symmetry of the continuum model usually provides a series of good quantum numbers to identify the modes namely the spheroidal and torsional vibrational modes. Therefore, despite being classical approach this produces the low-frequency Eigen values quite satisfactorily for the particles up to the sizes 4–5 nm on lower side. The elastic

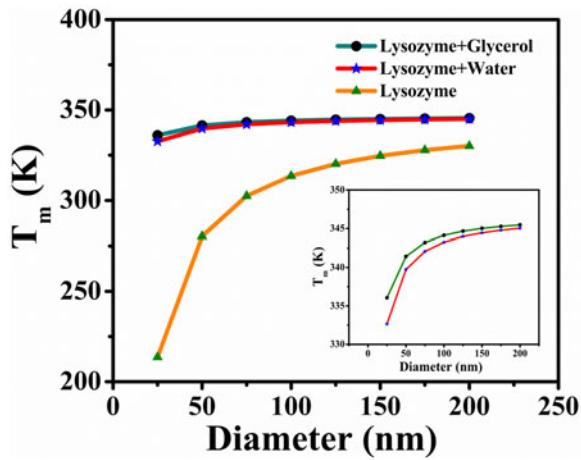


Figure 1. Size dependent melting temperature of free and embedded virus.

continuum model presents remarkable results for materials at nanoscale, providing a useful formulation for the approximate description of phonons and the technologically important carrier-phonon interactions in fullerenes and carbon nanotubes (Kahn, Kim, & Stroschio, 2001; Raichura, Dutta, & Stroschio, 2003). These elastic vibrations of spherical viruses overt themselves in the low-frequency Raman scattering spectra and requires theoretical understanding (Duval, 1992). Since the viruses are usually confined in some medium like water, air or any other aqueous medium, to ensure specific function of the virus particle the effect of surrounding medium- on low-frequency vibrations should be studied (Talati & Jha, 2006). However, the resulting vibrational mode frequencies in this case are complex numbers. While the real part reflects the Lamb's frequency, the nonzero imaginary part reflects the fact that the oscillatory motion is decaying in time due to flow of energy away from the vibrating nanoparticle (Talati & Jha, 2006). In this study, we use the temperature dependent low-frequency mode to determine the size dependent glass transition (T_g) of spherical virus. The determination of T_g has also been earlier achieved using Raman and Brillouin scattering in lysozyme with the objective to differentiate glass transition and dynamical transition (Khodadadi, Malkovskiy, Kisliuk, & Sokolov, 2010). The methodology to determine the low-frequency Raman vibrational modes in spherical virus has been discussed earlier by us in (Talati & Jha, 2006).

3. Results and discussion

This article reports the calculated results on the size- and medium-dependent thermodynamical properties melting temperature, catalytic activation energy and glass transition temperature of spherical virus. Figure 1 shows the size and matrix (water and glycerol) dependent melting temperature for spherical virus (lysozyme) which shows that the melting temperature rapidly decreases below 75-nm diameter similar to the other nanoparticles (Sun & Simon, 2007). The T_m of virus without any medium is almost constant above 175 nm and attains to the melting temperature of bulk lysozyme. We calculated melting temperature and presented in Table 1 together with the available experimental (Blanco, Ruso, Sabin, Prieto, & Sarmiento, 2007; Steinbach & Brooks, 1993)

and other theoretical (Katava et al., 2017) data. The obtained melting temperature of bulk lysozyme as 330 K is in good agreement with available experimental value obtained using differential scanning calorimetry (DSC) for chicken egg white lysozyme (CEWL) in the presence of perdeuterated matrices D_2O , glycerol and glucose (Katava et al., 2017). While the experimental melting temperature for CEWL hydrated with 0.4g water per gram of dry protein is 340 K, the same for CEWL embedded in 1:1 (gram protein per gram solvent) in glycerol and glucose is 370 K (Katava et al., 2017). However in the same work from stability curves, they found melting temperature for two systems as $T_{m,sim}^{wat} = 444 K$ and $T_{m,sim}^{gly} = 524K$ (Katava et al., 2017). This can be attributed to the convergence issues with atomistic force fields which generally overestimates the in silico melting temperature (Kresten, Piana, Dror, & Shaw, 2011).

Figure 1 also presents the size dependent melting temperature of spherical virus in two mediums water and glycerol, which shows a significant variation in the magnitude of melting temperatures as well as in the trend. Although there is an increase in melting temperature with size in the case of embedded virus, no rapid change is observed in melting temperature of embedded virus system. The melting temperature for both embedded systems at 200 K is about 25 K higher than the free virus, but the difference increases with lowering the temperature and is more than 100 K below 50 K. As far as two mediums glycerol and water are concerned the difference in melting temperature of virus is not very significant which can be seen from the inset of Figure 1. The melting temperature decrease of virus with size can be attributed to the increased surface-to-volume ratio of virus with its decreasing size (Allen, Bayles, Gile, & Jesser, 1986) and crystallinity of the structures (Koga, Ikeshoji, & Sugawara, 2004). However, when the virus is embedded in glycerol and water, the increase of melting temperature for a given size of virus can be attributed to the mismatch in the physical properties particularly the mechanical parameters and density of both virus particle and surrounding mediums (Talati & Jha, 2006). However, in the case of virus embedded in glycerol and water, the lower value of T_m in the case of water embedded virus can be attributed to the formation of stronger hydrogen bonds (Leslie, Israeli, Lighthart, Crowe, & Crowe, 1995) in polar water embedded viral protein and low cohesion energy due to less cohesion.

Figure 2 presents the size- and medium-dependent catalytic activation energy, E_a of considered spherical virus. The catalytic energy variation with size is similar to the melting temperature variation. All three curves representing three different cases show the decrease in E_a with decrease in size. The calculated catalytic activity energy for virus of about 200 nm (bulk) in all cases presented in Table 1 clearly shows a good agreement with previous results (Morozov & Gevorkian, 1985). In case of free virus the catalytic activation energy (E_a) is less than that of embedded virus. For water medium the catalytic activation energy is 89.2kj/mol for 25 nm virus which is higher than the same for 25 nm free virus. This comparison shows that the virus embedded in water has less catalytic activation energy than that of

Table 1. Table presents the calculated melting temperature, catalytic activity and glass transition for free and embedded virus along with the other studies.

System	Melting temperature (T_m , K)			Glass transition (T_g , K)			Catalytic activation energy (E_a , kJ/mol)	
	Present	Exp	Other theories (MD)	Present	Exp	Other theories (MD)	Present	Others
Lysozyme	330.1	340 ^a	–	191.55, (289.59)	130–240 ^b , 280–313 ^c , 200–220 ^d	220 ^e , 215–245 ^f	88.53	–
Lysozyme + water	345.03	347.95 ^g	444 ^h	(286.4)	150–170 ^b	–	92.52	75.3 ^b
Lysozyme + glycerol	345.45	349.15 ^g , 370 ^h	524 ^h	(281.3)	175 ^d , 220 ^e , 160–174 ^d	–	92.63	–

The bracket () number shows the glass transition T_g value from temperature dependence of the low-frequency phonon mode.

^aUsing spectroscopic techniques. (Blanco et al., 2007).

^bThrough viscoelastic properties studied at different hydration levels. (Morozov & Gevorkian, 1985).

^cUsing experimental techniques for the temperature-controlled optical studies of the biocrystals. (Teslyuk et al., 2007).

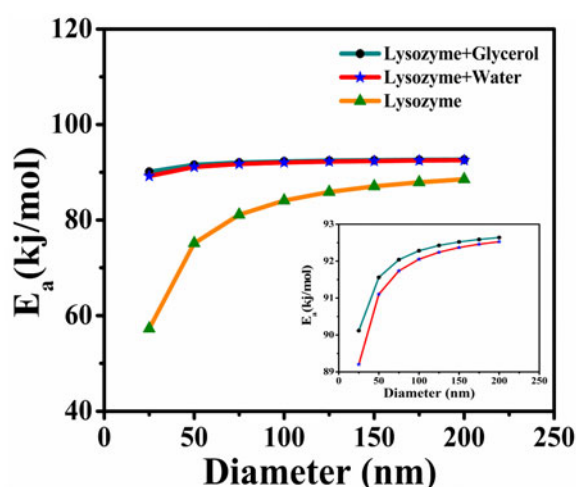
^dMyoglobin using dielectric spectroscopy and DSC (Jansson & Swenson, 2010).

^eGlass transition of myoglobin using molecular dynamic simulation (Steinbach & Brooks, 1993).

^fUsing equations based on Avramov's model (Monkos, 2015).

^gUsing CD and amide proton exchange monitored by two-dimensional ¹H NMR (Knubovets et al., 1999).

^hCombining both elastic incoherent neutron scattering and advanced molecular dynamic simulation. (Katava et al., 2017).

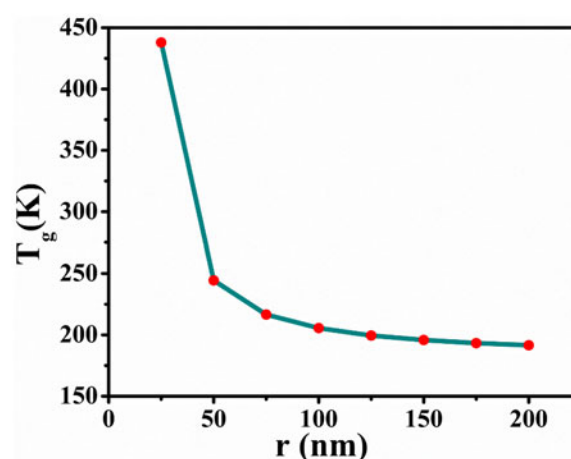
**Figure 2.** Size dependent catalytic activity of free and embedded virus.

glycerol medium and can be better in catalyzing any chemical reaction because less catalytic activation energy reveals to higher rate of chemical reaction.

However, it is important to note that the free virus has lower catalytic activation energy. The catalytic activation energy value will be almost equal above 200 nm size for both free and embedded cases.

Figures 3 and 4 show the calculated results on the size dependent glass transition temperature T_g using the expression based on thermodynamics and low-frequency Raman mode of spherical virus respectively. Figure 3 clearly depicts as size of virus increases there is a decrease in glass transition temperature T_g . It is interesting to note that the T_g/T_m ratio becomes more than one for the virus size of <50 nm in contrast to the usual trend in the polymer where it lies between 0.5 and 0.76 with a large majority of those with ratio 2:3 (Lee & Knight, 1970). This implies that the virus (material) behaves quite unsymmetrical for smaller size. However, for the size 150 nm the virus turns symmetrical as the T_g/T_m ratio is below 0.5 (Lee & Knight, 1970). This is in line of glass transition Lindemann criterion which shows $T_g \ll T_m$ (Dyre, 2006).

Table 1 clearly shows that the glass transition temperature for spherical virus composed of lysozyme protein is in good agreement with experimentally obtained values using DSC

**Figure 3.** Size dependent glass transition temperature of free virus.

and dielectric measurements (Jansson & Swenson, 2010; Morozov & Gevorkian, 1985; Steinbach & Brooks, 1993; Teslyuk, Vasylyk, Nastishin, & Vlokh, 2007) and other theoretical calculations (Monkos, 2015; Steinbach & Brooks, 1993). For the comparison we have also included data for myoglobin apart from the lysozyme which shows a good agreement between both. Figure 3b presents the temperature versus frequency of Raman active low-frequency spheroidal phonon mode. The low-frequency Raman active mode is calculated using continuum approach briefly discussed in above section due to its relative simplicity and ease of interpretation. In addition, the structure of spherical viruses is quite suitable to be used as a material in continuum model. Viruses are composed of individual coat proteins bundled together to be approximately like a sphere. Each individual coat protein in the bundle comprises several amino acids.

The calculation of properties using low-frequency mode based on elastic continuum model requires only two parameters, longitudinal and transverse sound velocities c_l and c_t , respectively of lysozyme as the measured speed of sound in different protein crystals is similar (Dykeman et al., 2007; Talati & Jha, 2006). Furthermore, the approximation of treating virus as perfect spheres is not a drawback for the lowest lying acoustic phonon modes which are the only once that we calculate and use for the determination of properties particularly

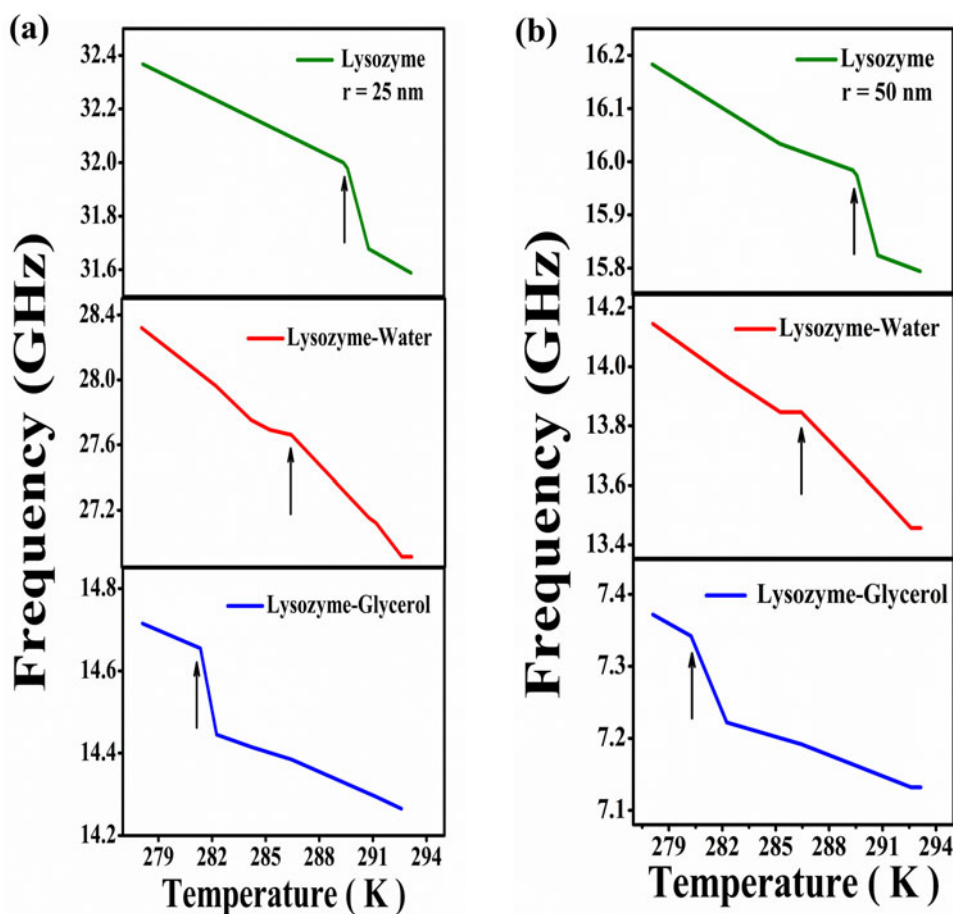


Figure 4. Temperature dependent low-frequency vibration curve for a free and embedded virus (a) for 25 nm and (b) 50 nm.

the glass transition temperature (Murray & Saviot, 2007). Furthermore, using the virus as homogeneous and isotropic object is justifiable as it has internal structure and without well-known anisotropy. It is clearly seen from the Figure 4 that the nature changes sharply indicating a sharp glass transition. The sharp change in the temperature dependence of the frequency of the low-frequency mode have been used earlier to estimate T_g in some glass formers (Forrest, Dalnoki-Veress, & Dutcher, 1997; Terki, Levelut, Prat, Boissier, & Pelous, 1997). However, the predicted value of T_g from temperature dependence of the low-frequency phonon mode is higher than the one obtained from thermodynamical calculation. This can be attributed to the fact that the low-frequency vibration is due to the whole vibration of the body. It is to be noted that the range of glass transition temperature which is obtained here is in good agreement with earlier measurements (Green, Fan & Angell, 1994; Morozov & Gevorkian, 1985; Sartor, Mayer, & Johari, 1994). However, when virus of 50 nm is embedded in medium such as water and glycerol, there is a decrease in T_g which may be attributed to the reduction in frequency due to damping of mode and radiating its vibrational energy to the water and glycerol.

4. Conclusion

This article presents the size dependent melting temperature, catalytic activation energy and glass transition temperature

of the spherical virus by considering this as lysozyme protein crystal. All considered parameters show temperature dependency. Although the melting temperature and catalytic activation energy increases with decreasing size the glass transition temperature shows reverse behavior. In all cases the respective parameters attain the bulk value. The melting temperature is the required temperature which can be used to denature and kill the virus of a particular size. The calculated catalytic activation energy of spherical virus may have the implications in the field of catalyst. The calculated value of T_g for virus can be used to determine the elasticity or mechanical properties of the virus and hence mimicking the actual condition. This study also shows the effect of glycerol and water on these properties. The surrounding medium increases the melting temperature and catalytic activity energy but decreases the glass transition temperature. The glass transition temperature of virus has also been calculated using the temperature dependent low-frequency vibrational mode which shows a consistent result. This study also brings out the potential of this technique to be used as a complementary technique for the determination of glass transition temperature of biological materials like virus and bacteria.

Acknowledgements

Authors are thankful to the Science and Engineering Research Board (SERB- SB/S2/CMP-0005/2013) and DST Indo-Poland (DST/INT/POL/P-33/2016) project for providing financial assistance.

Disclosure statement

No potential conflict of interest was reported by the authors.

References

- Aggarwal, A., May, E. R., Brooks, C. L., & Klug, W. S. (2016). Nonuniform elastic properties of macromolecules and effect of prestrain on their continuum nature. *Physical Review E*, 93(1), 012417. doi:10.1103/physreve.93.012417
- Allen, G. L., Bayles, R. A., Gile, W. W., & Jesser, W. A. (1986). Small particle melting of pure metals. *Thin Solid Films*, 144(2), 297–308. doi:10.1016/0040-6090(86)90422-0
- Alonso, J. M., Górzny, M. L., & Bittner, A. M. (2013). The physics of tobacco mosaic virus and virus-based devices in biotechnology. *Trends in Biotechnology*, 31(9), 530–538. doi:10.1016/j.tibtech.2013.05.013
- Arrhenius, S. (1889). Über die dissociationswärme und den einfluss der temperatur auf den dissociationsgrad der elektrolyte. *Zeitschrift Für Physikalische Chemie*, 4(1), 96–116. doi:10.1515/zpch-1889-0408
- Blanco, E., Ruso, J. M., Sabín, J., Prieto, G., & Sarmiento, F. (2007). Thermal stability of lysozyme and myoglobin in the presence of anionic surfactants. *Journal of Thermal Analysis and Calorimetry*, 87(1), 211–215. doi:10.1007/s10973-006-7842-5
- Chen, S., & Kucernak, A. (2004). Electrocatalysis under conditions of high mass transport rate: oxygen reduction on single submicrometer-sized Pt particles supported on carbon. *The Journal of Physical Chemistry B*, 108(10), 3262–3276. doi:10.1021/jp036831j
- Chung, W.-J., Oh, J.-W., Kwak, K., Lee, B. Y., Meyer, J., Wang, E., ... Lee, S.-W. (2011). Biomimetic self-templating supramolecular structures. *Nature*, 478(7369), 364–368. doi:10.1038/nature10513
- Dash, J. G. (1999). History of the search for continuous melting. *Reviews of Modern Physics*, 71(5), 1737–1743. doi:10.1103/RevModPhys.71.1737
- Dudowicz, J., Freed, K. F., & Douglas, J. F. (2005). The glass transition temperature of polymer melts. *The Journal of Physical Chemistry B*, 109(45), 21285–21292. doi:10.1021/jp0523266
- Duval, E. (1992). Far-infrared and Raman vibrational transitions of a solid sphere: Selection rules. *Physical Review B*, 46(9), 5795–5797. doi:10.1103/PhysRevB.46.5795
- Dykeman, E. C., Sankey, O. F., & Tsen, K. T. (2007). Raman intensity and spectra predictions for cylindrical viruses. *Physical Review E*, 76(1), 011906–011917. doi:10.1103/PhysRevE.76.011906
- Dyre, J. C. (2006). Colloquium: The glass transition and elastic models of glass-forming liquids. *Reviews of Modern Physics*, 78(3), 953–972. doi:10.1103/RevModPhys.78.953
- Farrant, J. (1970). Mechanisms of injury and protection in living cells and tissues at low temperatures. In A. U. Smith (Ed.), *Current trends in cryobiology* (p. 139). New York: Plenum; Tappel, A. L. (1966). In H. T. Meryman (Ed.), *Cryobiology* (p. 163). London: Academic.
- Flynn, C. E., Lee, S. W., Peelle, B. R., & Belcher, A. M. (2003). Viruses as vehicles for growth, organization and assembly of materials. *Acta Materialia*, 51(19), 5867–5880. doi:10.1016/j.actamat.2003.08.031
- Ford, L. H. (2003). Estimate of the vibrational frequencies of spherical virus particles. *Physical Review E*, 67, 051924. doi:10.1103/PhysRevE.67.051924
- Forrest, J. A., Dalnoki-Veress, K., & Dutcher, J. R. (1997). Interface and chain confinement effects on the glass transition temperature of thin polymer films. *Physical Review E*, 56(5), 5705–5716. doi:10.1103/PhysRevE.56.5705
- Ghavanloo, E., & Fazelzadeh, S. A. (2015). Nonlocal shell model for predicting axisymmetric vibration of spherical shell-like nanostructures. *Mechanics of Advanced Materials and Structures*, 22(7), 597–603. doi:10.1080/15376494.2013.828816
- Górzny, M., Walton, A. S., & Evans, S. D. (2010). Synthesis of high-surface-area platinum nanotubes using a viral template. *Advanced Functional Materials*, 20(8), 1295–1300. doi:10.1002/adfm.200902196
- Green, J. L., Fan, J., & Angell, C. A. (1994). The protein-glass analogy: New insight from homepeptide comparisons. *The Journal of Physical Chemistry*, 98(51), 13780–13790. doi:10.1021/j100102a052
- Gupta, S. K., Sahoo, S., Jha, P. K., Arora, A. K., & Azhniuk, Y. M. (2009). Observation of torsional mode in CdS_{1-x}Se_x nanoparticles in a borosilicate glass. *Journal of Applied Physics*, 106(2), 024307–024314. doi:10.1063/1.3171925
- Gupta, S. K., Talati, M., & Jha, P. K. (2008). Shape and size dependent melting point temperature of nanoparticles. *Materials Science Forum*, 570, 132–137. doi:10.4028/www.scientific.net/MSF.570.132
- Jackson, C. L., & McKenna, G. B. (1991). The glass transition of organic liquids confined to small pores. *Journal of Non-Crystalline Solids*, 131–133(1), 221–224. doi:10.1016/0022-3093(91)90305-P
- Jansson, H., & Swenson, J. (2010). The protein glass transition as measured by dielectric spectroscopy and differential scanning calorimetry. *Biochimica et Biophysica Acta - Proteins and Proteomics*, 1804(1), 20–26. doi:10.1016/j.bbapap.2009.06.026
- Jerome, B. (1999). Dynamics of glass-forming materials confined in thin films. *Journal of Physics: Condensed Matter*, 11(10A), A189–A197. doi:10.1088/0953-8984/11/10A/014
- Jiang, Q., & Yang, C. C. (2008). Size effect on the phase stability of nanostructures. *Current Nanoscience*, 4(2), 179–200. doi:10.2174/157341308784340949
- Jiang, Q., Shi, H. X., & Li, J. C. (1999). Finite size effect on glass transition temperatures. *Thin Solid Films*, 354(1–2), 283–286. doi:10.1016/S0040-6090(99)00537-4
- Kahn, D., Kim, K. W., & Stroschio, M. A. (2001). Quantized vibrational modes of nanospheres and nanotubes in the elastic continuum model. *Journal of Applied Physics*, 89(9), 5107. doi:10.1063/1.1356429
- Katava, M., Stirnemann, G., Zanatta, M., Capaccioli, S., Pachetti, M., Ngai, K. L., ... Paciaroni, A. (2017). Critical structural fluctuations of proteins upon thermal unfolding challenge the Lindemann criterion. *Proceedings of the National Academy of Sciences of the United States of America*, 114(35), 9361–9366. doi:10.1073/pnas.1707357114
- Khodadadi, S., Malkovskiy, A., Kisliuk, A., & Sokolov, A. P. (2010). A broad glass transition in hydrated proteins. *Biochimica et Biophysica Acta - Proteins and Proteomics*, 1804(1), 15–19. doi:10.1016/j.bbapap.2009.05.006
- Koga, K., Ikeshoji, T., & Sugawara, K. I. (2004). Size- and temperature-dependent structural transitions in gold nanoparticles. *Physical Review Letters*, 92(11), 115507–115511. doi:10.1103/PhysRevLett.92.115507
- Koh, Y. P., McKenna, G. B., & Simon, S. L. (2006). Calorimetric glass transition temperature and absolute heat capacity of polystyrene ultrathin films. *Journal of Polymer Science Part B: Polymer Physics*, 44(24), 3518–3527. doi:10.1002/polb.21021
- Kresten, L. L., Piana, S., Dror, R. O., & Shaw, D. E. (2011). How fast-folding proteins fold. *Science*, 334(6055), 517–520. doi:10.1126/science.1208351
- Ku, T., Lu, P., Chan, C., Wang, T., Lai, S., Lyu, P., & Hsiao, N. (2009). Predicting melting temperature directly from protein sequences. *Computational Biology and Chemistry*, 33(6), 445–450. doi:10.1016/j.compbiolchem.2009.10.002
- Lamb, H. (1882). On the Vibrations of an Elastic Sphere. *Proceedings of the London Mathematical Society*, 1, 189–212. doi:10.1112/plms/s1-14.1.50
- Lee, W. A., & Knight, G. J. (1970). Ratio of the glass transition temperature to the melting point in polymers. *British Polymer Journal*, 2(1), 73–80. doi:10.1002/pi.4980020112
- Leslie, S. B., Israeli, E., Lighthart, B., Crowe, J. H., & Crowe, L. M. (1995). Trehalose and sucrose protect both membranes and proteins in intact bacteria during drying. *Applied and Environmental Microbiology*, 61(10), 3592–3597. URL: <https://aem.asm.org/content/61/10/3592>.
- Lošdorfer Božič, A., & Šiber, A. (2018). Electrostatics-driven inflation of elastic icosahedral shells as a model for swelling of viruses. *Biophysical Journal*, 115(5), 822–829. doi:10.1016/j.bpj.2018.07.032
- Lu, H. M., & Meng, X. K. (2010). Morin temperature and Néel temperature of hematite nanocrystals. *The Journal of Physical Chemistry C*, 114(49), 21291–21295. doi:10.1021/jp108703b
- Mallamace, F., Corsaro, C., Mallamace, D., Vasi, S., Vasi, C., Baglioni, P., ... Stanley, H. E. (2016). Energy landscape in protein folding and unfolding. *Proceedings of the National Academy of Sciences of the United States of America*, 113(12), 3159–3163. doi:10.1073/pnas.1524864113

- Mamedov, K. K., Abdullaev, A. B., Shalumov, B. Z., Mekhtiev, M. I., Alyanov, M. A., & Gumbatov, D. O. (1987). Low-temperature heat capacity and thermodynamic properties of silicon-dioxide-based binary vitreous systems. *Physica Status Solidi (A)*, 99(2), 413–421. doi:10.1002/pssa.2210990211
- May, E. R. (2014). Recent developments in molecular simulation approaches to study spherical virus capsids. *Molecular Simulation*, 40(10-11), 878–888. doi:10.1080/08927022.2014.907899
- Monkos, K. (2015). Determination of the glass-transition temperature of proteins from a viscometric approach. *International Journal of Biological Macromolecules*, 74, 1–4. doi:10.1016/j.ijbiomac.2014.11.029
- Morozov, V. N., & Gevorkian, S. G. (1985). Low-temperature glass transition in proteins. *Biopolymers*, 24(9), 1785–1799. doi:10.1002/bip.360240909
- Murray, D. B., & Saviot, L. (2007). Damping by bulk and shear viscosity for confined acoustic phonons of a spherical virus in water. *Journal of Physics: Conference Series*, 92(1), 012036–012040. doi:10.1088/1742-6596/92/1/012036
- Nanda, K. K. (2009). Size-dependent melting of nanoparticles: Hundred years of thermodynamic model. *Pramana*, 72(4), 617–628. doi:10.1007/s12043-009-0055-2
- Pankhurst, Q. A., Connolly, J., Jones, S. K., & Dobson, J. (2003). Applications of magnetic nanoparticles in biomedicine. *Journal of Physics D: Applied Physics*, 36(13), R167–R181. doi:10.1088/0022-3727/36/13/201
- Park, H., Heldman, N., Rebentrost, P., Abbondanza, L., Iagatti, A., Alessi, A., ... Belcher, A. M. (2016). Enhanced energy transport in genetically engineered excitonic networks. *Nature Materials*, 15(2), 211–216. doi:10.1038/nmat4448
- Pauling, L. (1948). Nature of forces between large molecules of biological interest. *Nature*, 161(4097), 707–709. doi:10.1038/161707a0
- Qi, W. H., & Wang, M. P. (2005). Size- and shape-dependent superheating of nanoparticles embedded in a matrix. *Materials Letters*, 59(18), 2262–2266. doi:10.1016/j.matlet.2004.06.079
- Raichura, A., Dutta, M., & Strocio, M. A. (2003). Quantized acoustic vibrations of single-wall carbon nanotube. *Journal of Applied Physics*, 94(6), 4060. doi:10.1063/1.1600846
- Sartor, G., Mayer, E., & Johari, G. P. (1994). Calorimetric studies of the kinetic unfreezing of molecular motions in hydrated lysozyme, hemoglobin, and myoglobin. *Biophysical Journal*, 66(1), 249–258. doi:10.1016/S0006-3495(94)80774-X
- Shenton, W., Douglas, T., Young, M., Stubbs, G., & Mann, S. (1999). Inorganic-organic nanotube composites from template mineralization of tobacco mosaic virus. *Advanced Materials*, 11(3), 253–256. doi:10.1002/(SICI)1521-4095(199903)11:3 < 253::AID-ADMA253 > 3.0.CO;2-7
- Shi, F. G. (1994). Size dependent thermal vibrations and melting in nanocrystals. *Journal of Materials Research*, 9(5), 1307–1314. doi:10.1557/JMR.1994.1307
- Siepi, M., Politi, J., Dardano, P., Amoresano, A., De Stefano, L., Monti, D. M., & Notomista, E. (2017). Modified denatured lysozyme effectively solubilizes fullerene c60 nanoparticles in water. *Nanotechnology*, 28(33), 335601–335616. doi:10.1088/1361-6528/aa744e
- Steinbach, P. J., & Brooks, B. R. (1993). Protein hydration elucidated by molecular dynamics simulation. *Proceedings of the National Academy of Sciences of the United States of America*, 90(19), 9135–9139. doi:10.1073/pnas.90.19.9135
- Stillinger, F. H., & Stillinger, D. K. (1990). Computational study of transition dynamics in 55-atom clusters. *Journal of Chemical Physics*, 93(8), 6013–6024. doi:10.1063/1.459488
- Sun, J., & Simon, S. L. (2007). The melting behavior of aluminum nanoparticles. *Thermochimica Acta*, 463(1–2), 32–40. doi:10.1016/j.tca.2007.07.007
- Talati, M., & Jha, P. K. (2006). Acoustic phonon quantization and low-frequency Raman spectra of spherical viruses. *Physical Review E*, 73(1), 011901–011907. doi:10.1103/PhysRevE.73.011901
- Terki, F., Levelut, C., Prat, J. L., Boissier, M., & Pelous, J. (1997). Low-frequency dynamics in an optical strong glass: Vibrational and relaxational contributions. *Journal of Physics: Condensed Matter*, 9(19), 3955–3971. doi:10.1088/0953-8984/9/19/015
- Teslyuk, I., Vasyukiv, Y., Nastishin, Y., & Vlokh, R. (2007). Structural phase transition in lysozyme crystals. *Ferroelectrics*, 346(1), 49–55. doi:10.1080/00150190601180216
- Tsen, K. T., Dykeman, E. C., Sankey, O. F., Lin, N. T., Tsen, S. W., & Kiang, J. G. (2006). Observation of the low frequency vibrational modes of bacteriophage M13 in water by Raman spectroscopy. *Virology Journal*, 3(1), 79–90. [Mismatch] doi:10.1186/1743-422X-3-79
- Zhang, C. Y., & Zhang, N. H. (2018). Influence of Microscopic Interactions on the Flexible Mechanical Properties of Viral DNA. *Biophysical Journal*, 115(5), 763–772. doi:10.1016/j.bpj.2018.07.023
- Zheng, K., Lu, M., Liu, Y., Chen, Q., Taccardi, N., Hüser, N., & Boccaccini, A. R. (2016). Monodispersed lysozyme-functionalized bioactive glass nanoparticles with antibacterial and anticancer activities. *Biomedical Materials*, 11(3), 035012–035025. doi:10.1088/1748-6041/11/3/035012
- Zhong, C., Wang, Y., Ma, G., & Li, R. (2016). Measurement of the onset temperature of irreversible inactivation of proteins using FITC as a fluorescent reporter. *Analytical Methods*, 8(18), 3809–3815. doi:10.1039/C5AY03234B
- Zhou, Y., Vitkup, D., & Karplus, M. (1999). Native proteins are surface-molten solids: Application of the Lindemann criterion for the solid versus liquid state. *Journal of Molecular Biology*, 285(4), 1371–1375. doi:10.1006/jmbi.1998.2374



Influence of size, shape and dimension on glass transition and Kauzmann temperature of silver (Ag) and tantalum (Ta) nanoparticles

Chetna S. Tiwari · Arun Pratap · Prafulla K. Jha

Received: 5 February 2020 / Accepted: 15 July 2020
© Springer Nature B.V. 2020

Abstract A simple model is developed for the investigation of size, shape and dimension dependent glass transition temperature (T_g) and Kauzmann temperature (T_K) of nanoparticles. The model is based on thermodynamical quantity cohesive energy and is free from fitting parameters and approximations. To check the validity of the model, calculations on the size, shape and dimension dependent glass transition (T_g) and Kauzmann temperature (T_K) are performed for silver (Ag) and tantalum (Ta) nanoparticles (NPs) of different shapes. The considered shapes are spherical, tetrahedral, octahedral and icosahedral accompanied with zero-, one- and two-dimensional geometries. Our results reveal that the T_g and T_K strongly depend on the size of the nanoparticles. As the size of the NPs decreases, T_g and T_K decrease. It is observed that both temperatures follow the trend as (icosahedral, D) > (spherical, D) > (octahedral, D) > (tetrahedral, D) for selected Ag and Ta nanoparticles. However, in terms of dimension, they show the $d=0 < d=1 < d=2$ trend. The calculated values of glass transition and Kauzmann temperatures for both considered nanoparticles have good agreement with available

molecular dynamics (MD) simulation and experimental data.

Keywords Glass transition temperature · Kauzmann temperature · Metal nanoparticles · Shape · Size

Introduction

The size effects on materials exhibit unique physical, chemical and mechanical properties and lead to a variety of applications such as catalysis, sensors, photochemistry and optoelectronics [Chen and Mao 2007; Seifert 2004; Narayanan and El-Sayed 2003]. It is observed that reducing the size or dimension of glassy material results into several unusual and useful mechanical behaviours [Zhong et al. 2014; Luo et al. 2016; Sun et al. 2014; Yu et al. 2013; Yu Yu et al. 2015]. Metallic glasses have a significant role in different fields of science due to their applications in small-scale devices, such as nano-electromechanical systems, biomedical implants, precision microparts, surgical tools and micro machines [Kumar et al. 2011]. The first metallic glass was produced in 1960 by Duwez and coworkers by rapidly cooling a molten alloy of gold and silicon [Khan et al. 2017]. The metallic glasses are broadly classified into two categories: (i) the metal-metalloid glasses and (ii) the metal-metal glasses. One of the emerging classes of metallic glass is monoatomic metallic glass. However, the glassy behaviour of monoatomic metallic liquids is not yet efficiently explored. The liquid-glass transition phenomenon is observed in various types of liquids,

C. S. Tiwari · A. Pratap
Department of Applied Physics, Faculty of Technology and Engineering, The Maharaja Sayajirao University of Baroda, 390002, Vadodara, India

P. K. Jha (✉)
Department of Physics, Faculty of Science, The Maharaja Sayajirao University of Baroda, 390002, Vadodara, India
e-mail: prafullaj@yahoo.com

such as molecular, ionic, metallic, oxide and chalcogenide liquids [Kauzmann 1948; Debenedetti and Stillinger 2001; Gibbs and Di Marzio 1958; Sastry et al. 1998; Krakoviack 2005; Scala et al. 2000; Sastry 2001; Tanaka 2005]. Literature reveals that the verification of monoatomic metallic liquids is extremely difficult. However, Zhong et al. [2014] achieved an unprecedentedly high quenching rate of 10^{14} K/s in nanoscale materials and vitrified the monoatomic metallic liquids on the extremely small nano-tips [Zhong et al. 2014]. The verification of a super cooled liquid is often understood in terms of glass transition temperature (T_g) and the corresponding Kauzmann temperature (T_K). In a thermodynamic view of the glass transition, an ideal thermodynamic second-order transition should take place from a supercooled liquid to a glass with a single conformation at (T_K) [Kauzmann 1948; Debenedetti and Stillinger 2001; Gibbs and Di Marzio 1958; Ao et al. 2007; Adam and Gibbs 1965]. The Kauzmann temperature represents a temperature, below which the transitional molecular motions responsible for major physical and chemical changes in materials can be negligible in the normal product timescales [Jiang et al. 1997; Stillinger et al. 1999; Coluzzi et al. 2000], and is always less than glass transition. As a result, T_K can be helpful to know the maximum temperature for storing the glasses. Previous studies show that the T_g and T_K are size and dimension dependent thermodynamical parameters [Ao et al. 2007; Mishra et al. 2012; Bhatt et al. 2012]. Theoretical as well as, experimental methods have been employed to establish the relation between $T_g(D)$ and melting temperature $T_m(D)$ [Alcoulabi and McKenna 2005; Jiang and Lang 2004]. Furthermore, MD simulation has been employed to show that the $T_K(D)$ of selected size will be lower than the bulk T_K [Attili et al. 2005]. However, due to kinetic restrictions, it is difficult to measure direct experimental data for T_K . However, it can be indirectly determined by extrapolation from experimental data based on some theoretical models, such as the Vogel-Fulcher law with viscosity measurements [Jiang et al. 1997; Klose and Fecht 1994; Saslow 1988] and Kauzmann [Kauzmann 1948].

The metallic nanoparticles such as silver (Ag), gold (Au) and tantalum (Ta) have a special place in nanomaterial research due to their potential applications in digital circuits, biotechnology and catalysts [Gao et al. 2007; Morones et al. 2005]. The tantalum nanoparticles particularly have significant applications in

superconductors, orthopaedic implants, dopants in photo electrode materials and micro-batteries [Wang et al. 2004]. Due to the difficulty in experimental setup, theoretical models as well as MD simulations can be used to evaluate the glass transition and Kauzmann temperatures. Theoretical models to determine these temperatures can be developed using cohesive energy expression due to linear relationship between them. Among them, a number of cohesive energy models work only for spherical nanoparticles [Nanda et al. 2002; Guisbiers and Wautelet 2006; Safaei et al. 2008; Guisbiers et al. 2008]. However, they cannot be used for nanoparticles of any other shape except sphere without any modification. In addition, several size and shape dependent models have been proposed, but they require a lot of input parameters from literature or experimental work [Kumar and Kumar 2012; Guisbiers 2010]. However, in the lack of these data, the model adapts several fitting parameters or approximations for the calculations [Bhatt and Kumar 2017].

In this work, we have formulated a simple model to investigate size, shape and dimension dependent glass transition temperature (T_g) and Kauzmann temperature (T_K) by employing cohesive energy expression, which is free from fitting parameters and requires minimum input data which are easily available from literature. Furthermore, thermal behaviour of silver and tantalum nanoparticles for spherical, icosahedral, octahedral and tetrahedral shapes are studied and accompanied with $d = 0$, $d = 1$ and $d = 3$ dimensions.

Methodology

Melting of a solid is a phase transition from solid to liquid state by absorbing heat energy. This phenomenon becomes dramatic for nanoparticles due to increased surface to volume ratio. The melting initiates from surface due to less cohesive energy of the surface atoms as compared with interior atoms. Each atom shares a bond with neighbouring atoms. This bond provides cohesive energy; hence, atoms with fewer bonds and neighbouring atoms have lower cohesive energy. Therefore, cohesive energy of nanoparticle can be expressed as the sum of energies contributed by interior atoms and the surface atoms as [Qi 2005]

$$nE_c(D) = E_c(\infty)(n-N) + \frac{1}{2} E_c(\infty)N \quad (1)$$

where n , $(n - N)$ and N represent the number of total atoms, interior atoms and surface atoms of the nanoparticles, respectively, and $E_c(D)$ and $E_c(\infty)$ represent the cohesive energy of nanoparticle for selected size and corresponding bulk material, respectively. Equation (1) can also be written as

$$E_c(D) = E_c(\infty) \left(1 - \frac{N}{2n} \right) \tag{2}$$

where N/n ratio represents the surface to volume ratio of atoms and thus varies with shapes. The surface atoms, N , and total number of atoms, n , of a nanoparticle can be calculated as [Lu et al. 2009]

$$\frac{N}{n} = \frac{\frac{N_1}{n_1}}{\frac{N_2}{n_2}} \tag{3}$$

where

$$N_1 = \frac{\text{surface area of selected shape}}{\text{surface area of atoms}}, N_2 = \frac{\text{surface area of spherical shape with } D_0}{\text{surface area of atoms}}, \tag{4}$$

$$n_1 = \frac{\text{volume of selected shape}}{\text{volume of atoms}}, n_2 = \frac{\text{volume of spherical shape with } D_0}{\text{volume of atoms}}$$

On further simplification,

$$\frac{N}{n} = \frac{\text{surface area of selected shape}}{\text{volume of selected shape}} * \frac{\text{volume of spherical or 1D or 2D shape with } D_0}{\text{surface area of spherical or 1D or 2D shape with } D_0}$$

where D_0 is the critical size where all the atoms of the nanocrystal are located on the surface. The relation between atomic diameter (h) and dimension (d) can be expressed in terms of critical diameter expression as $D_0 = 2(3-d)h$ [Lu et al. 2009]; (i) $D_0 = 6h$ for nanoparticles with dimension $d = 0$, since $4\pi r_0^2 h = \frac{4}{3}\pi r_0^3$ (ii) $D_0 = 4h$ for cylindrical nanowires with $d = 1$, since $2\pi r_0 h = \pi r_0^2$ and (iii) $D_0 = 2h$ for thin films with $d = 2$, since $2h = 2r_0$. Here, r_0 is the critical radius where all the atoms of the nanocrystal are located on the surface. This makes N/n ratio a shape and dimension dependent parameter. Crystals always possess a characteristic of long-range order, and according to Jiang et al. [Jiang et al. 1999], the smallest nanocrystal should have at least a half of the atoms located within the nanocrystal. Hence, the smallest size r of nanoparticle is $2r_0$ which is equal to D_0 . This estimation was found consistent with the available experimental results for Bi film and Pb nanowire in a carbon nanotube [Jiang et al. 1999]. Thus, D_0 is an important parameter which explains that no particles with $r < 2r_0$ can exist in the crystalline state and will assist to understand the thermodynamical properties of nanocrystal in appropriate way.

For a nanoparticle, D is considered a diameter for spherical shape and edge/length/thickness for non-spherical shapes. For a spherical nanoparticle with diameter D , its volume will be $\pi D^3/6$, and the atomic volume will be $\pi h^3/6$, where h is the atomic diameter. Then, total number of atoms can be obtained as $n_1 = (\pi D^3/6) / (\pi h^3/6)$. However, further simplification makes $n_1 = D^3/h^3$. Surface area of a spherical nanoparticle with diameter D is πD^2 , and as each surface atom contributes to the surface area of the nanoparticle, the area of the great circle of the atom will be $\pi h^2/4$ [Qi 2005]. For calculating the total number of surface atoms, we get $N_1 = (\pi D^2) / (\pi h^2/4)$ which further turns as $N_1 = 4D^2/h^2$. As a result the ratio of N_1 and n_1 for spherical nanoparticle will be $N_1/n_1 = 4h/D$. Similarly, n_2 will represent the total number of atoms within size D_0 of spherical nanoparticle, i.e. $n_2 = D_0^3/h^3$, and N_2 represents the surface atoms of spherical nanoparticle with size D_0 as $N_2 = 4D_0^2/h^2$. Hence, the ratio of surface to volume for D_0 size can be expressed as $N_2/n_2 = 4h/D_0$. Thus, $N/n = D_0/D$ which on further substitution with $D_0 = 6h$ for nanoparticle can be written as $6h/D$. For regular tetrahedral-shaped nanoparticle, $N_1 = \frac{\sqrt{3}D^2}{\pi h^2/4}$, $n_1 =$

$\frac{\sqrt{2}D^3/12}{\pi h^3/6}$ and $N_2/n_2 = 4h/D_0$, and on further substitution, $N/n = \sqrt{6} D_0/D$. By replacing the value of $D_0 = 6h$, $N/n = 6\sqrt{6} h/D \approx 14.7h/D$. For regular icosahedral-shaped nanoparticle, $N_1 = (\sqrt{75} D^2) / (\frac{\pi h^2}{4})$, $n_1 = [5(3 + 51/2)D_3/12] / (\pi h^3/6)$ and $N_2/n_2 = 4h/D_0$, so we get $N/n \approx 3.96h/D$ with $D_0 = 6h$. For regular octahedral-shaped nanoparticle, $N_1 = (121/2D_2) / (\frac{\pi h^2}{4})$, $n_1 = (21/2D_3/3) / (\pi h^3/6)$ and $N_2/n_2 = 4h/D_0$. In case of spherical, cubical, tetrahedral, octahedral and icosahedral nanostructures, $d = 0$, and hence $D_0 = 6h$ [Lu et al. 2009]. For cylindrical nanowire, $N_1 = (\pi D l) / (\frac{\pi h^2}{4})$, $n_1 = (\pi D 2l / 4) / (\pi h^3/6)$, $N_2 = (\pi D_0 l) / (\frac{\pi h^2}{4})$ and $n_2 = (\pi D_0 2l / 4) / (\pi h^3/6)$; hence, $N/n = D_0/D$. As nanowire falls in the $d = 1$ category, i.e. one dimensional, so $D_0 = 4h$ resulting $N/n = 4h/D$. For a rectangular geometry thin film, the surface area will be length multiplied by the width of the film. Volume will be surface area multiplied by thickness. $N_1 = (lb) / (\frac{\pi h^2}{4})$, $n_1 = (lbD) / (\pi h^3/6)$, $N_2 = (lb) / (\frac{\pi h^2}{4})$, $n_2 = (lbD_0) / (\pi h^3/6)$, hence $N/n = D_0/D$. Substituting $d = 2$ for thin films, $D_0 = 2h$ and hence $N/n = 2h/D$, where D is the thickness of thin film. The calculated values of surface to volume ratio for various shapes are shown in Table 1.

Here, h/D is the ratio of atomic diameter to the selected diameter/length/thickness of the nanoparticle. This ratio varies from selected material to material. The linear relationship of cohesive energy, melting temperature and glass transition temperature with bond strength [Mishra et al. 2012; Qi 2005] leads to

$$\frac{E_c(D)}{E_c(\infty)} = \frac{T_m(D)}{T_m(\infty)} = \frac{T_g(D)}{T_g(\infty)} = \left(1 - \frac{N}{2n}\right) \tag{5}$$

As T_K cannot be measured experimentally, we have obtained a relation between T_K and T_m (melting temperature) using Kauzmann theory. Moreover, T_K is also called the entropy crisis temperature where entropy of liquid and its crystalline counterpart is the same [Kauzmann 1948].

$$S_m(T_K) = S_L(T_K) - S_S(T_K) = 0 \tag{6}$$

where $S_m(T)$ denotes temperature dependent melting entropy and the subscripts m, l and s represent the

Table 1 Comparison of N/n values between present model and Qi's model for different shapes

Shapes	Present model	Qi's model
Spherical	$6h/D$	$4h/D$
Cubic	$6h/D$	$4h/D$
Tetrahedral	$14.7h/D$	$9.79h/D$
Octahedral	$7.38h/D$	$4.89h/D$
Icosahedral	$3.96h/D$	$2.64h/D$
Cylindrical nanowire	$4h/D$	$2.66h/D$
Thin films	$2h/D$	$1.33h/D$

melting, liquid, and crystal transition, respectively. Equation (6) can be modified using the temperature dependent Gibbs free energy difference between liquid and the crystal in bulk as

$$G_m(T, \infty) = \frac{7TH_m(\infty)[T_m(\infty) - T]}{T_m(\infty)[T_m(\infty) + 6T]} \tag{7}$$

where $H(\infty)$ and $T_m(\infty)$ represent the bulk melting enthalpy and bulk melting temperature. Equation (7) which is experimentally verifiable [Ao et al. 2007] predicts that the $G_m(T, \infty)$ reaches its maximum value at T_K and when $dG_m(T, \infty)/dT_{T=T_K} = 0$. Thus, we obtain Kauzmann temperature for bulk material as

$$T_K(\infty) = \left[\left(\sqrt{7}-1\right)/6\right] T_m(\infty) \tag{8}$$

However, at nanoscale, Eq. (7) can be written as [Ao et al. 2007]

$$G_m(T, D) = \frac{7TH_m(D)[T_m(D) - T]}{T_m(D)[T_m(D) + 6T]} \tag{9}$$

The condition $dG_m(T, \infty)/dT_{T=T_K} = 0$ gives the Kauzmann temperature with selected size as

$$T_K(D) = \left[\left(\sqrt{7}-1\right)/6\right] T_m(D) \tag{10}$$

Further, comparing Eq. (8) and Eq. (10), we get

$$\frac{T_K(D)}{T_K(\infty)} = \frac{T_m(D)}{T_m(\infty)} \tag{11}$$

Equations (5) and (11) provide the relation between E_c , T_K and T_g in terms of melting temperature T_m as

$$\frac{E_c(D)}{E_c(\infty)} = \frac{T_m(D)}{T_m(\infty)} = \frac{T_K(D)}{T_K(\infty)} = \frac{T_g(D)}{T_g(\infty)} = \left(1 - \frac{N}{2n}\right) \quad (12)$$

The Kauzmann and glass temperatures of a material can be easily calculated for selected size, shape and dimension using Eq. (12). Using experimentally available bulk melting temperature, $T_K(\infty)$ can be calculated using Eq. (8), while $T_g(\infty)$ is obtained from references [Ao et al. 2007; Li et al. 2017].

Results and discussion

Figure 1 depicts the size dependent Kauzmann temperature calculated using Eq. (5) for Ag nanoparticles. This figure also presents the data from MD simulation and Qi’s model [Ao et al. 2007; Qi 2005]. The calculated values obtained using Eq. (12) are found in better correspondence with the MD simulation results [Ao et al. 2007] than Qi’s model. This can be attributed to the introduction of critical diameter in the cohesive energy expressions. It is clearly seen from the figure that the Kauzmann temperature decreases with decrease in size. Significant drop in T_K is seen for $D < 5$ nm due to increased surface to volume ratio. As a result, when size increases, the value of Kauzmann temperature approaches towards bulk Kauzmann temperature. Further, the variation in Kauzmann temperature (T_K) with size for different dimension is calculated for Ag nanoparticles and presented in Fig. 2. It can be seen from Fig. 2 that the T_K decreases with decrease in size as

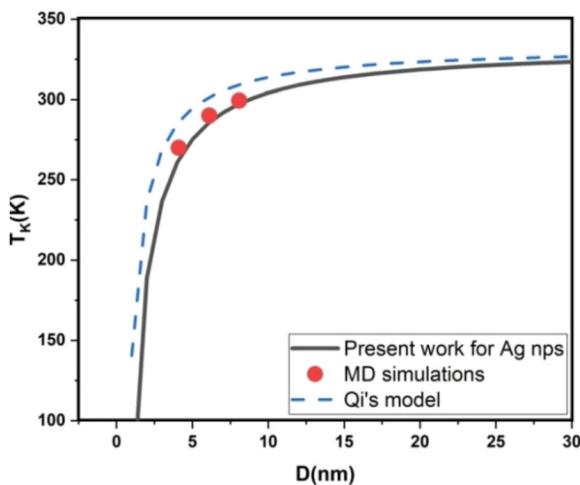


Fig. 1 Size dependent Kauzmann temperature for Ag nanoparticles

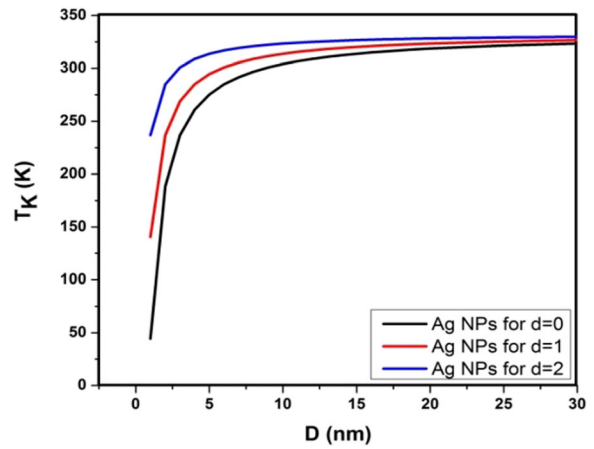


Fig. 2 Size and dimension dependent Kauzmann temperature for Ag nanoparticles

well as dimension. However, for the constant size, the trend in T_K is observed as $T_K(d = 2) > T_K(d = 1) > T_K(d = 0)$. But this discrimination in T_K for different dimensions declines with increase in nanoscale size (Table 2).

Our model predicts the value of $T_K(\infty) / T_m(\infty) \approx 0.27$ for Ag nanoparticles which is consistent with the value of 0.2–0.3 for metallic elements [Ao et al. 2007]. A size-independent T_K/T_m is interpreted with constant size effect on both T_K and T_m induced specifically by surface to volume ratio which also promotes that the intrinsic melting mechanism is independent of crystalline size and found consistent with Lindeman’s melting criterion [Ao et al. 2007]. We now turn our attention to the variation in glass transition temperature for Ag nanoparticles of different shapes. Figure 3 presents the variation of T_g with shape and size. It is observed that the icosahedral-shaped Ag nanoparticle shows the highest T_g and tetrahedral-shaped Ag nanoparticle shows the least T_g with constant size.

The sequence of T_g is follows: $T_g(\text{icosahedral}) > T_g(\text{spherical}) > T_g(\text{octahedral}) > T_g(\text{tetrahedral})$. The number of atoms on various sites varies from shape to shape which in turn alters the coordination number of the atoms on the surface and thus is responsible for the

Table 2 Input parameters for calculations

Metallic nanoparticle	Atomic diameter (nm)	$T_m(\infty)$ (K)	$T_K(\infty)$ (K)	$T_g(\infty)$ (K)
Ag	0.289	1235	333	750
Ta	0.292	3290	888	1754

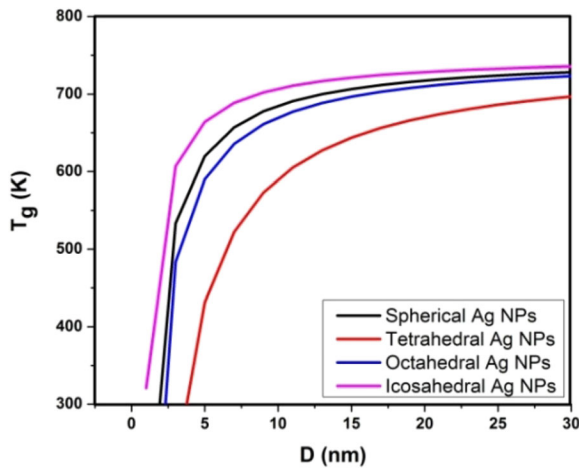


Fig. 3 Size and shape dependent glass transition temperature (T_g) of silver (Ag) nanoparticles

difference for the selected size. It is noteworthy that the equilibrium shape for fcc Ag clusters is truncated octahedral [Baletto et al. 2002].

Figure 4 shows the effect of size and dimensions on T_g of Ag nanoparticles using Eq. (12). Due to difference in the values of N/n ratio for spherical ($d=0$), nanowire ($d=1$) and nano films ($d=2$) variation in the glass transition temperatures is observed. Table 1 clearly reveals that as N/n ratio of different dimensions decreases, T_g value of Ag nanoparticles increases with size.

Figure 5 shows the variation in temperatures of Ag nanoparticles as a function of size (D). Among the three temperatures, it is observed that the temperatures for a nanoparticles of selected size follow the sequence $T_m(D) > T_g(D) > T_K(D)$. All three temperatures show

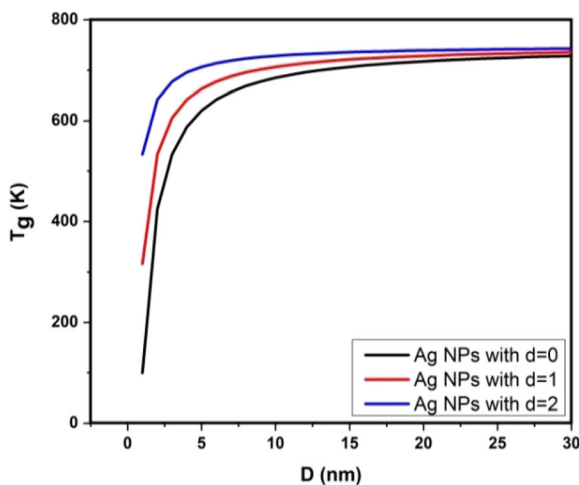


Fig. 4 Size (D) and dimension (d) dependent silver (Ag) nanoparticles

similar characteristics and significant drop in temperatures for $D < 5$ nm. This indicates that the dynamics in the supercooled liquid region becomes much faster with a decreasing droplet size so that in contrast to bulk liquids, liquid droplets with smaller sizes can only be frozen into glassy states in a much lower temperature region.

It is clear from Fig. 6 that the glass temperature T_g of Ta nanoparticles decreases with size, similar to the case of Ag nanoparticles. The calculated values are also compared with MD simulation data [Li et al. 2017] and Qi's model [Qi 2005]. Our model is found more consistent than Qi's model with MD simulation data for $D < 7$ nm. For $D > 7$ nm, a deviation between calculated values and MD simulations is observed. Furthermore, we observe a rapid drop in glass transition temperature of Ta nanoparticles like Ag nanoparticles for $D < 7$ nm due to increased surface to volume ratio. A major divergence in the curves between present work and Qi's model is observed between size 5 nm to 10 nm in case of T_g . When the size of nanomaterials decreases, several microscopic and quantum size effects dominate, such as the transformation of lattice structure and higher dissociation energies at the electronic shell-closing [Zhang et al. 2018]. As a result slight deviation is observed between our results and MD simulation data in the range < 4 nm because of ignorance of the quantum size effect and change in structure. Figure 7 depicts the glass transition temperature of Ta nanoparticles for different dimensions $d=0$, $d=1$ and $d=2$. We found that the $T_g(d=0) < T_g(d=1) < T_g(d=2)$ for selected size of Ta nanoparticles which is similar in nature with Fig. 4

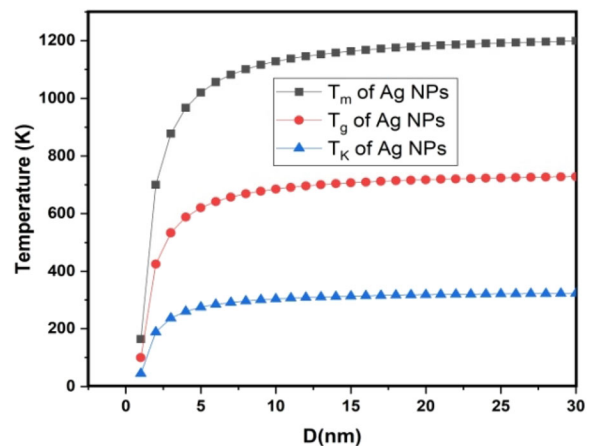


Fig. 5 Variation in melting, glass and Kauzmann temperature of Ag nanoparticles as a function of size (D)

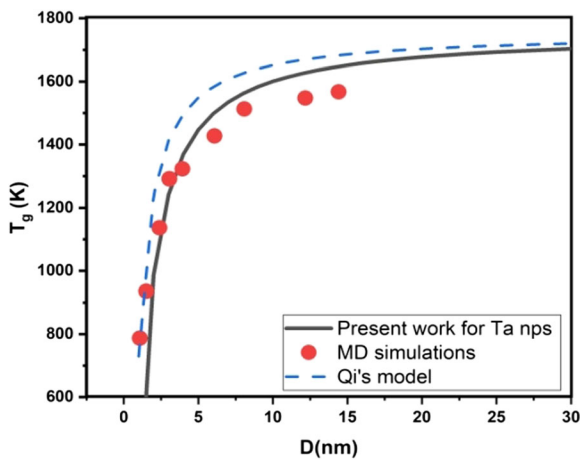


Fig. 6 Size (D) dependent glass transition (T_g) temperature of tantalum nanoparticles

within thermodynamical limit. Here, thermodynamic limit reveals the range of size in which a prominent decrease in selected quantity can be observed. Further, the observed trend in the variation of T_g with different dimensions can be attributed to the atoms on the surface, edges and corners.

The variation in T_K with respect to size in terms of shapes and dimensions are presented in Fig. 8 and Fig. 9. Figure 10 clearly shows that the tetrahedral shape has a minimum and icosahedral shape and has a maximum value of T_K for the selected size. To understand this, we have plotted size dependent surface to volume ratio and N/n ratio for all shaped Ta and Ag nanoparticles.

It is observed from Fig. 10 that the temperatures for Ta nanoparticles vary with size (D). All the three

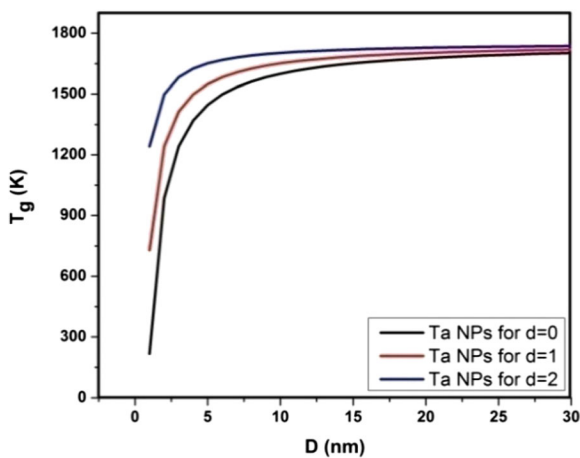


Fig. 7 Size and dimension dependent glass transition temperature (T_g) of Ta nanoparticles

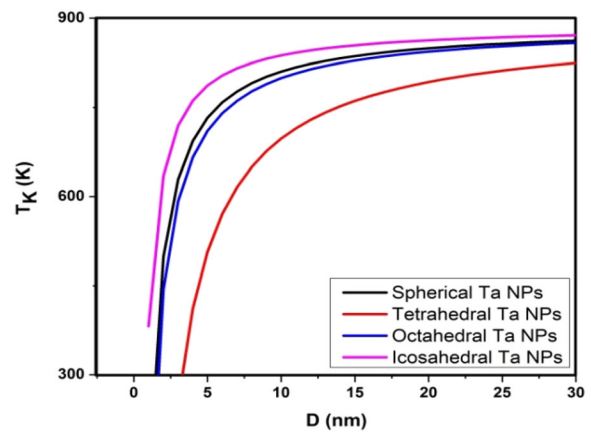


Fig. 8 Size dependent glass Kauzmann temperature (T_K) of Ta nanoparticles

temperatures for Ta nanoparticles are found in close proximity for $D > 3$ nm, but as the size increases, the temperatures diverge from each other. Glass transition temperature of Ta nanoparticles is found intermediate among melting and Kauzmann temperatures. This graph can be a useful tool to measure the Kauzmann and glass transition temperatures in experimental setup.

Figure 11 demonstrates the surface to volume ratio of atoms (N_1/n_1) for icosahedral, spherical, octahedral and tetrahedral shapes with inverse diameter (D^{-1}) for Ag and Ta nanoparticles. Among the selected shapes, the icosahedral-, spherical- and octahedral-shaped nanoparticles are seen in close vicinity, while tetrahedral-shaped nanoparticles are observed at a distant position with reference to the rest of the shapes. Hence, it is clear that (N_1/n_1) (tetrahedral) $>$ (N_1/n_1) (octahedral) $>$ (N_1/n_1) (spherical) $>$ (N_1/n_1) (icosahedral) for constant nanosize

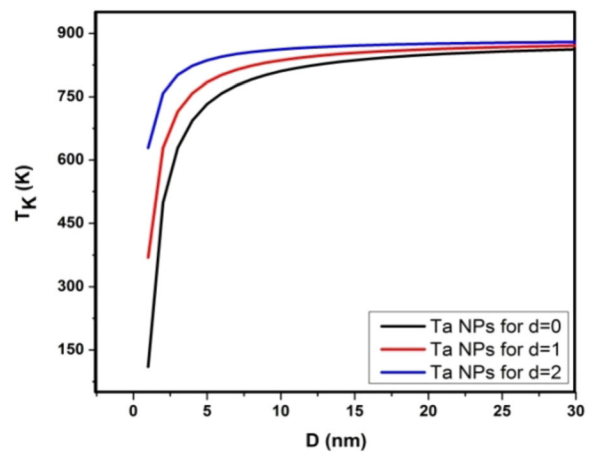


Fig. 9 Size and dimension dependent glass Kauzmann temperature (T_K) of Ta nanoparticles

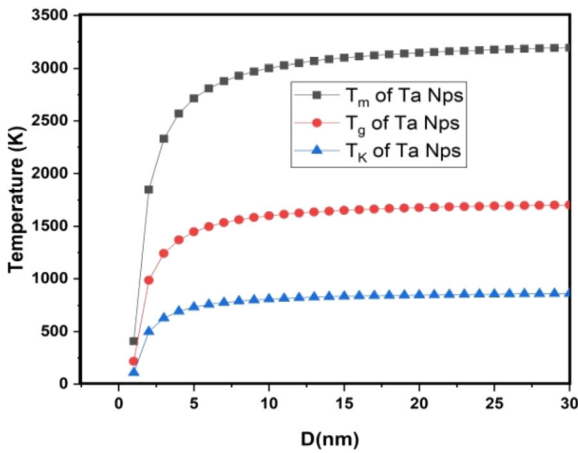


Fig. 10 Variation in melting, glass and Kauzmann temperature of Ta nanoparticles as a function of size (D)

of Ag and Ta nanoparticles. As ratio of atoms for tetrahedral shape is highest which in turn shows maximum availability of atoms on surface and thus results into least melting, glass transition and Kauzmann temperatures among other shapes for selected nanosize [Lu et al. 2009]. In case of different shaped nanoparticles, prominent ratio of surface to volume atoms can be seen for $D^{-1} > 0.14 \text{ nm}^{-1}$ or $D < 7 \text{ nm}$ for both materials. Beyond this size, the ratio of atoms gradually approaches to the constant value irrespective of selected shape and material.

Figure 12 presents the dimension dependent surface to volume ratio of atoms for Ag and Ta nanoparticles. As shown in Fig. 10, surface to volume ratio of atoms follows the sequence as (N_1/n_1) (nanosphere) $>$ (N_1/n_1)

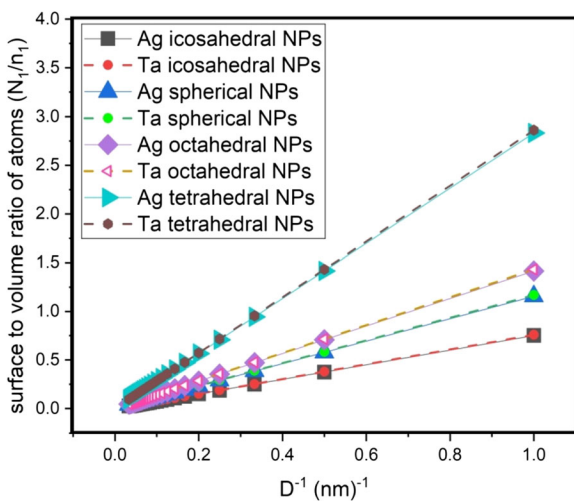


Fig. 11 Comparison of surface to volume ratio of atoms (N_1/n_1) for different shapes with inverse size (D^{-1}) for Ag and Ta NPs

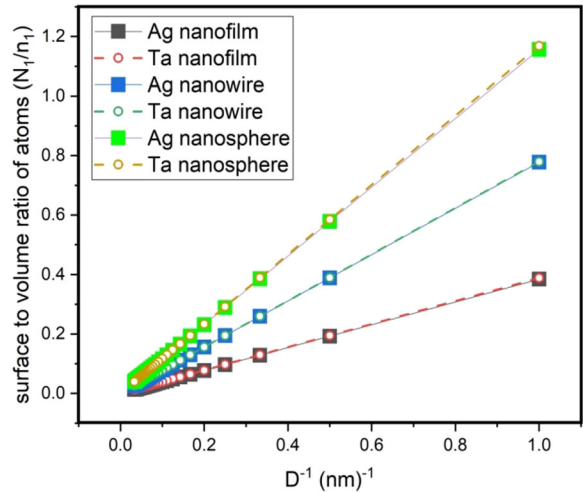


Fig. 12 Comparison of surface to volume ratio of atoms (N_1/n_1) for different dimensions with inverse size (D^{-1}) for Ag and Ta NPs

(nanowire) $>$ (N_1/n_1) (nanofilm) for nanoparticles of both Ag and Ta, which in turn demonstrates the highest availability of atoms on surface for nanosphere (0-d) and hence results into least glass transition and Kauzmann temperatures among other dimensions and can be confirmed from Figs. 2, 4, 6 and 8 for both Ag and Ta nanoparticles. The ratio of atoms nearly coincides for Ag and Ta nanoparticles for selected size, shape and dimension on the basis of close proximity in their atomic diameter with a difference of $\approx 0.003 \text{ nm}$ and is evident from Figs. 9 and 10.

Based on the above analysis, it is clear that the atoms in the surface layer possess much faster dynamics than those in the interior of selected shaped nanoparticles [Li et al. 2017]. As a result with decreasing size, the surface layer plays more and more important roles in the dynamical and mechanical properties of the nanoparticles.

Conclusions

We have calculated the size, shape and dimension dependent glass transition and Kauzmann temperatures for Ag and Ta nanoparticles using a simple model. This model has served our purpose in terms of temperatures with input parameters like bulk temperature, atomic diameter and surface to volume ratio of the selected material which are easily available. Our model is free from any assumptions, fitting parameters and approximations. During the investigation, we found that the temperatures decrease with decrease in size (D) and

dimension (d) due to increased surface to volume ratio. Our predictions using a simple model show good agreement with the available MD simulated data in both the cases. For selected nanosize, shape and dimension, we observed the series of temperatures as $T_m(D) > T_g(D) > T_K(D)$. In case of $d=0$, both glass transition and Kauzmann temperature follow the sequence as (icosahedral, D) > (spherical, D) > (octahedral, D) > (tetrahedral, D) for the selected nanoparticle. While in terms of dimensions, they are just reversed, i.e. $d=0 < d=1 < d=2$, for the selected size and metallic nanoparticles. These results are obtained on the ground of surface to volume ratio, which in turn shows the availability of atoms on surface. Higher surface to volume ratio will result into least melting temperatures within nanosize. Thus, we conclude that the shape and dimension can be effective only within thermodynamic limit of a few nm and gradually the impact of these parameters on any thermodynamical properties declines with increase in size. These conclusions can be fruitful for potentially manipulating the properties of metallic liquids and glasses within the scale of nanometre.

Funding information Authors are thankful to the Science and Engineering Research Board (SERB-SB/S2/CMP-0005/2013) for providing financial assistance.

Compliance with ethical standards

Conflict of interest The authors declare that they have no conflict of interest.

References

- Adam G, Gibbs JH (1965) On the temperature dependence of cooperative relaxation properties in glass-forming liquids. *J Chem Phys* 43:139–146
- Alcoutlabi M, McKenna GB (2005) Effects of confinement on material behaviour at the nanometre size scale. *J Phys: Condens Matter* 17:461
- Ao ZM, Zheng WT, Jiang Q (2007) Size effects on the Kauzmann temperature and related thermodynamic parameters of Ag nanoparticles. *Nanotechnology* 18:255706–255712
- Attili A, Gallo P, Rovere M (2005) Inherent structures and Kauzmann temperature of confined liquids. *Phys. Rev E* 71: 031204
- Baletto F, Ferrando R, Fortunelli A, Montalenti F, Mottet C (2002) Crossover among structural motifs in transition and noble-metal clusters. *J Chem Phys* 116:3856–3863
- Bhatt P, Pratap A, Jha PK (2012) Study of size-dependent glass transition and Kauzmann temperatures of tin dioxide nanoparticles. *J Therm Anal Calorim* 110:535–538
- Chen X, Mao SS (2007) Titanium dioxide nanomaterials: synthesis, properties, modifications, and applications. *Chem Rev* 107:2891–2959
- Coluzzi B, Parisi G, Verrocchio P (2000) Thermodynamical liquid-glass transition in a Lennard-Jones Binary Mixture. *Phys Rev Lett* 84:306–309
- Debenedetti PG, Stillinger FH (2001) Supercooled liquids and the glass transition. *Nature* 410:259–267
- Guisbiers G (2010) Size-dependent materials properties toward a universal equation. *Nanoscale Res. Lett.* 5:1132–1136
- Gao W, Zhao M, Jiang Q (2007) A DFT study on electronic structures and catalysis of $\text{Ag}_{12}\text{O}_6/\text{Ag}(111)$ for ethylene epoxidation. *J Phys Chem C* 111:4042–4046
- Gibbs JH, Di Marzio EA (1958) Nature of the glass transition and the glassy state. *J Chem Phys* 28:373–383
- Guisbiers G, Kazan M, Van Overschelde O, Wautelet M, Pereira S (2008) Mechanical and thermal properties of metallic and semiconductive nanostructures. *J Phys Chem C* 112:4097–4103
- Guisbiers G, Wautelet M (2006) Size, shape and stress effects on the melting temperature of nano-polyhedral grains on a substrate. *Nanotechnology* 17:2008–2011
- Jiang Q, Lang XY (2004) Glass transition of low-dimensional polystyrene. *Macromol. Rapid Commun* 25:825
- Jiang Q, Zhao M, Xu XY (1997) Kauzmann temperature of alloys obtained by different methods. *Phil Mag B* 76:1–10
- Kauzmann W (1948) The nature of the glassy state and the behaviour of liquids at low temperatures. *Chem Rev* 43: 219–256
- Khan MM, Nemati A, Rahman ZU, Shah UH, Asgar H, Haider W (2017) Recent advancements in bulk metallic glasses and their applications: a review. *Critical Reviews In Solid State and Materials Sciences* 43:233–268
- Klose G, Fecht HJ (1994) Vitrification close to the Kauzmann point of eutectic Au Pb Sb alloys. *Mater. Sci. Eng. A* 180:77–80
- Krakoviack V (2005) Liquid-glass transition of a fluid confined in a disordered porous matrix: a mode-coupling theory. *Phys Rev Lett* 94:065703–065707
- Kumar G, Desai A, Schroers J (2011) Bulk metallic glass: the smaller the better. *Adv. Mater.* 23:461–476
- Li YZ, Sun YT, Lu Z, Li MZ, Bai HY, Wang WH (2017) Size effect on dynamics and glass transition in metallic liquids and glasses. *J Chem Phys* 146:224502
- Lu HM, Li PY, Cao ZH, Meng XK (2009) Size-, Shape-, and Dimensionality-Dependent Melting Temperatures of Nanocrystals. *J Phys Chem C* 113:7598–7602
- Luo J, Wang J, Bitzek E, Huang JY, Zhang H, Tong L, Yang Q, Li J, Mao SX (2016) Size-dependent brittle-to-ductile transition in silica glass nanofibers. *Nano Lett* 16:105–113
- Mishra S, Jha PK, Pratap A (2012) Study of size-dependent glass transition and Kauzmann temperature of titanium dioxide nanoparticles. *J Therm Anal Calorim* 107:65–68
- Morones J et al (2005) The bactericidal effect of silver nanoparticles. *Nanotechnology* 16:2346
- Nanda KK, Sahu SN, Behera SN (2002) Liquid drop model for the size-dependent melting of lowdimensional systems. *Phys. Rev. A* 66, 013208
- Narayanan R, El-Sayed MA (2003) Effect of catalysis on the stability of metallic nanoparticles: Suzuki reaction catalyzed

- by PVP-palladium nanoparticles. *J Am Chem Soc* 125:8340–8347
- Jiang Q, Shi HX, Zhao M (1999) Melting thermodynamics of organic nanocrystals. *J Chem Phys* 111:5
- Kumar R, Kumar M (2012) Effect of size on cohesive energy, melting temperature and Debye temperature of nanomaterial. *Indian J pure Appl. Phys.* 50:329–334
- Bhatt S, Kumar M (2017) Effect of size and shape on melting and superheating of free standing and embedded nanoparticles. *J Phys Chem Solids* 106:112–117
- Safaei A, Shandiz M, Sanjabi A, Barber S, Z. H. (2008) Modeling the melting temperature of nanoparticles by an analytical approach. *J Phys Chem C* 112:99–155
- Saslow WS (1988) Scenario for the Vogel-Fulcher “law”. *Phys Rev B* 37:676–678
- Sastry S (2001) The relationship between fragility, configurational entropy and the potential energy landscape of glass-forming liquids. *Nature* 409:164–167
- Sastry S, Debenedetti PG, Stillinger FH (1998) Signatures of distinct dynamical regimes in the energy landscape of a glass-forming liquid. *Nature* 393:554–557
- Scala A, Starr FW, Nave EL, Sciortino F, Stanley HE (2000) Configurational entropy and diffusivity of supercooled water. *Nature* 406:166–175
- Seifert G (2004) Nanocluster magic. *Nat Mater* 3:77–78
- Stillinger FH et al (1999) *J Phys Chem B* 103:7390
- Sun J, He LB, Lo YC, Xu T, Bi HC, Sun L, Zhang Z, Mao SX, Li J (2014) Liquid-like pseudo-elasticity of sub-10-nm crystalline silver particles. *Nat Mater* 13:1007–1012
- Tanaka H (2005) Two-order-parameter model of the liquid–glass transition. III. Universal patterns of relaxations in glass-forming liquids. *J Non-Cryst Solids* 351:3396–3413
- Qi WH (2005) Size effect on melting temperature of nanosolids. *Physica B* 368(2005):46–50
- Wang Y et al (2004) Synthesis and phase structure of tantalum nanoparticles. *Mater Lett* 58:3017–3020
- Yu HB, Luo Y, Samwer K (2013) Ultrastable metallic glass. *Adv Mater* 25:5904–5908
- Yu HB et al (2015) Suppression of β relaxation in vapor-deposited ultrastable glasses. *Phys Rev Lett* 115:185501–185506
- Zhang X et al (2018) Size and shape dependent melting temperature of metallic nanomaterials *J. Phys: Condens Matter* 31:7
- Zhong L, Wang J, Sheng H, Zhang Z, Mao SX (2014) Formation of monatomic metallic glasses through ultrafast liquid quenching. *Nature* 512:177–180

Publisher’s note Springer Nature remains neutral with regard to jurisdictional claims in published maps and institutional affiliations.